Toward Isolated Molecular Wires: A pH-Responsive Canopied Polypyrrole

Dongwhan Lee† and Timothy M. Swager*

Department of Chemistry, Massachusetts Institute of Technology, 77 Massachusetts Avenue, Cambridge, Massachusetts 02139

Received April 15, 2005

The design, synthesis, and electropolymerization of sterically hindered pyrrole derivatives are described. Endo and exo adducts of cyclopentadiene and *N*-phenylmaleimide were converted to give bicyclo[2.2.1]-heptane-fused pyrrole monomers, in which a phenyl group is rigidly placed proximate the pyrrole fragment. Oxidative polymerization of these monomers affords highly conductive polypyrroles. The rigid molecular scafffold of the pyrrole monomers limits cross-communication between adjacent conducting strands and produces a defined narrow potential window of high conductivity dominated by intrachain polaronic charge carriers. The resultant loosely packed polymer chains allow for superior sensory properties. Notably, the electrical conductivity of oxidatively doped poly(**7**) could be reversibly modulated in aqueous electrolytes at pH 3−9.

Introduction

Conjugated organic materials have long been considered efficient low-dimensional charge-carrying conduits.[1−3] The unique spectroscopic, electrochemical, and electrical conduction properties associated with these extended chemical architectures are readily exploited for sensing applications.[4,5] We have had a long-standing interest in the design of sensors wherein only a few chemical events produce a perturbation in the energy landscape of the conjugated polymer (CP) system that affects the mobility of the charge-carrying species.[6,7] Mechanisms that are particularly effective involve analyte-induced reductions in conjugation length of the CP backbone or induced energy mismatches between adjacent redox-active sites.[5,8] The result is a reduced conductivity of the bulk material, which can be readily and precisely determined by simple resistance measurements.[9,10]

Synthetic efforts directed at the design of new CP sensors have mainly targeted optimizing host−guest chemistry, as it plays a pivotal role in enhancing *specificity*. Indeed, CPs with elaborated receptors have been shown to display excellent binding affinities toward specific targets.[5] Equally crucial in the context of amplification is a precise control over the conduction pathways traversed by the charge-carrying species, as this property dictates the *sensitivity* of the system. As depicted in Scheme 1, amplification of the signal arising from local binding events in resistivity-based sensors relies on blocking of the specific pathway for charge migration. For an idealized one-dimensional (1D) CP strand spanning two electrodes (Scheme 1, top), deconjugation elicited by analyte binding effectively "cuts" the molecular wire.[4] The result is a complete shutdown of charge conduction. Despite such a desirable signal transduction with a high signal-to-noise ratio, it is difficult to fabricate this structure *in mass* from conventional CP-based sensory materials. In addition to the inherent structural inhomogeneity associated with direct electrodeposition of the bulk CP materials, $\pi-\pi$ stacking interactions are generally present between adjacent

Scheme 1. Idealized One- and Two-Dimensional Charge Hopping in CP and Its Perturbation Leading to Resistivity-Based Sensing

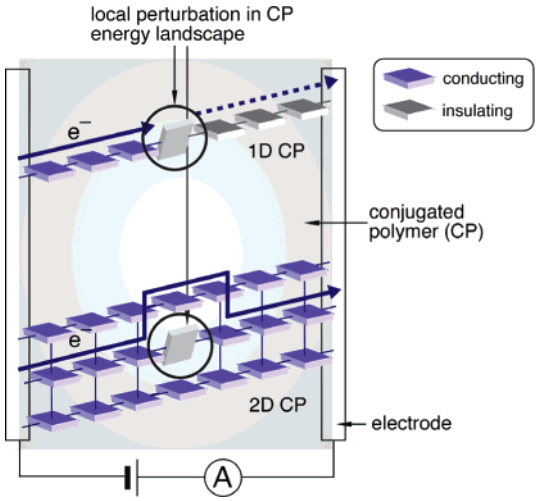

* To whom correspondence should be addressed. E-mail: tswager@mit.edu.
† Present address: Department of Chemistry, Indiana University, Bloomington, IN 47405.

(1) *Electronic Materials: The Oligomer Approach*; Müllen, K., Wegner, G., Eds.; Wiley-VCH: New York, 1998.
(2) *Organic Electronic Materials: Conjugated Polymers and Low Molecular Weight Organic Solids*; Farchioni, R., Grosso, G., Eds.; Springer: Berlin, 2001.
(3) Special Issue on Organic Electronics. *Chem. Mater.* **2004**, *16*, No. 23.
(4) Swager, T. M. *Acc. Chem. Res.* **1998**, *31*, 201−207.
(5) McQuade, D. T.; Pullen, A. E.; Swager, T. M. *Chem. Rev.* **2000**, *100*, 2537−2574.
(6) Wosnick, J. H.; Swager, T. M. *Curr. Opin. Chem. Biol.* **2000**, *4*, 715−720.
(7) Lee, D.; Swager, T. M. *Synlett* **2004**, 149−154.
(8) Holliday, B. J.; Swager, T. M. *Chem. Commun.* **2005**, 23−36.
(9) Kittlesen, G. P.; White, H. S.; Wrighton, M. S. *J. Am. Chem. Soc.* **1984**, *106*, 7389−7396.
(10) Ofer, D.; Crooks, R. M.; Wrighton, M. S. *J. Am. Chem. Soc.* **1990**, *112*, 7869−7879.

10.1021/cm050803r CCC: $30.25 © 2005 American Chemical Society
Published on Web 08/06/2005

Scheme 2. Defining One-Dimensional Conduits for Charge Conduction

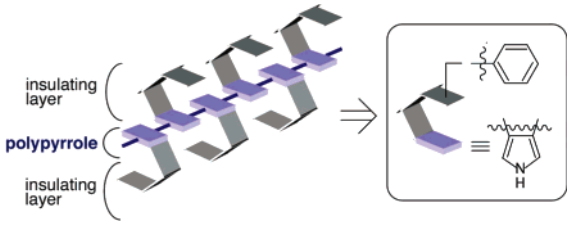

polymer backbones, thereby providing multiple hopping or delocalization pathways for the charge-carrying species (Scheme 1, bottom).[7] Within these typical π-stacked three-dimensional (3D) electronic networks, charge carriers encountering a local analyte-induced energy barrier can readily find alternative routes to traverse the distance between the two electrodes. Hence the carrier's path between the electrodes is lengthened but not blocked, which significantly compromises sensitivity. An ideal solution for this challenge is to use chemical structures that define a limited number of charge-transporting pathways within the bulk material by minimizing cross-communication between CP strands.[11]

In the quest for chemical architectures that intrinsically enforce reduced dimensionality, we were attracted to pyrrole derivatives shrouded with electro*in*active groups arranged in a rigid 3D structure about the polymer backbone. This structural consideration was expected to prevent interstrand $\pi-\pi$ stacking interactions in the resulting polymer (Scheme 2).[7,12−15] The highly porous internal structure afforded by an ensemble of such canopied polypyrrole strands should also facilitate inclusion of guest molecules,[16] as has previously been demonstrated by poly(phenyleneethynylenes) built on sterically demanding pentiptycene-derived platforms,[17] and triptycene-appended dye molecules aligned within liquid crystal hosts.[18]

In this contribution, we present a full description of our synthetic efforts to control charge-transporting pathways within CPs.[19] Conformationally well-defined bicyclo[2.2.1]-heptane-fused pyrrole derivatives were prepared and electrochemically polymerized to afford highly conductive materials. The importance of the precise structural control was demonstrated by examining two different polymers obtained from compositionally identical but stereochemically distinctive isomers. Our findings are that only the canopied polypyrrole derivative provided a reversibe pH response in aqueous media. A tight coupling between CP redox chemistry and acid−base chemistry facilitated a rapid switching of the conductivity. This process is assisted by the restricted charge hopping pathways defined within the bulk material.

Experimental Section

General Considerations. All reagents were obtained from commercial suppliers and used as received unless otherwise noted. Dichloromethane and tetrahydrofuran (THF) were saturated with nitrogen and purified by passage through activated Al_2O_3 columns under nitrogen.[20] The compound *tert*-butyl α-isocyanoacetate was prepared according to literature procedures.[21]

Physical Measurements. ^{1}H NMR and ^{13}C NMR spectra were recorded on a Varian Mercury 300 MHz spectrometer. High-resolution mass spectra (HR-MS) were obtained on a Bruker Daltronics APEX II 3 Tesla FT-ICR-MS. Chemical shifts were reported versus tetramethylsilane and referenced to the residual solvent peaks. Fourier transform infrared (FT-IR) spectra were recorded on a Nicolet Impact 410 instrument with OMNIC software. Solid samples were pressed into KBr pellets. UV−vis spectra were recorded on a Hewlett-Packard 8452A diode array spectrophotometer.

2-*endo*,6-*endo*-4-Phenyl-4-azatricyclo[5.2.1.0^{2,6}]dec-8-ene-3,5-dione (1). To a rapidly stirred intense yellow solution of *N*-phenylmaleimide (5.00 g, 28.9 mmol) in CH_2Cl_2/Et_2O (1:1, 40 mL) at 0 °C was added dropwise freshly distilled cyclopentadiene (2.5 mL, 37 mmol). The reaction mixture was warmed to room temperature and stirred for 1 h. The color of the solution gradually faded. Volatile fractions were removed and the residual solid was triturated with Et_2O. Off-white crystalline solid of **1** (6.40 g, 93%) was isolated by filtration and dried in vacuo. mp 137 °C. ^{1}H NMR (300 MHz, $CDCl_3$): δ 7.46−7.33 (m, 3H), 7.15−7.12 (m, 2H), 6.26 (dd, 2H, apparent t), 3.52−3.48 (m, 2H), 3.42 (dd, 2H, J = 3.0 and 1.8 Hz), 1.79 (dt, 1H, J = 9.0 and 1.7 Hz), 1.61 (d, 1H, J = 9.0 Hz). ^{13}C NMR (75 MHz, $CDCl_3$): δ 176.7, 134.6, 131.8, 129.1, 128.6, 126.6, 52.4, 45.9, 45.6. IR (KBr, cm^{-1}) 3058, 3000, 2947, 1768, 1714, 1498, 1375, 1337, 1189, 846, 743, 719. HR-MS (ESI) calcd for $C_{15}H_{13}NO_2Na$ [M + Na]$^+$ 262.0844, found 262.0836.

(±)-8-Chloro-4-phenyl-9-phenylsulfanyl-4-azatricyclo[5.2.1.0^{2,6}]-decane-3,5-dione (2). To a rapidly stirred anhydrous CH_2Cl_2 (10 mL) suspension of *N*-chlorosuccinimide (1.27 g, 9.51 mmol) under Ar was added dropwise thiophenol (0.85 mL, 8.3 mmol). The reaction was initiated by gentle heating, and the resulting orange suspension was subsequently placed in an ice bath during the addition. The heterogeneous mixture was warmed to room temperature, stirred for 0.5 h, and cooled at −78 °C. A CH_2Cl_2 solution (7 mL) of **1** (1.98 g, 8.27 mmol) was added over a period of 5 min. The mixture was warmed to room temperature and stirred overnight under Ar. Volatile fractions were removed and the residual oily material was purified on silica (hexanes:EtOAc = 2:1) to provide an off-white solid of **2** (2.86 g, 90%). mp 188 °C. ^{1}H NMR (300 MHz, $CDCl_3$): δ 7.52−7.23 (m, 10H), 4.17 (m, 1H), 3.57−3.49 (m, 2H), 3.39 (m, 1H), 3.28 (m, 1H), 2.95 (m, 1H), 2.24 (d, 1H, J = 10.1 Hz), 1.85 (d, 1H, J = 11.1 Hz). ^{13}C NMR (75 MHz, $CDCl_3$): δ 175.5, 174.8, 134.3, 132.0, 129.37, 129.35, 129.3, 128.9, 126.9, 126.6, 63.4, 53.4, 48.8, 47.7, 46.2, 46.1, 40.6. IR (KBr, cm^{-1}) 3056, 2983, 1772, 1710, 1498, 1483, 1376, 1181, 741, 692. HR-MS (ESI) calcd for $C_{21}H_{18}NO_2ClNaS$ [M + Na]$^+$ 406.0645, found 406.0639.

(11) Buey, J.; Swager, T. M. *Angew. Chem., Int. Ed.* **2000**, *39*, 608−612.
(12) Cornil, J.; Beljonne, D.; Calbert, J.-P.; Brédas, J.-L. *Adv. Mater.* **2001**, *13*, 1053−1067.
(13) Cacialli, F.; Wilson, J. S.; Michels, J. J.; Daniel, C.; Silva, C.; Friend, R. H.; Severin, N.; Samorí, P.; Rabe, J. P.; O'Connell, M. J.; Taylor, P. N.; Anderson, H. L. *Nat. Mater.* **2002**, *1*, 160−164.
(14) Cardin, D. J. *Adv. Mater.* **2002**, *14*, 553−563.
(15) van den Boogaard, M.; Bonnet, G.; van't Hof, P.; Wang, Y.; Brochon, C.; van Hutten, P.; Lapp, A.; Hadziioannou, G. *Chem. Mater.* **2004**, *16*, 4383−4385.
(16) Budd, P. M.; Ghanem, B. S.; Makhseed, S.; McKeown, N. B.; Msayib, K. J.; Tattershall, C. E. *Chem. Commun.* **2004**, 230−231.
(17) Yang, J.-S.; Swager, T. M. *J. Am. Chem. Soc.* **1998**, *120*, 11864−11873.
(18) Long, T. M.; Swager, T. M. *J. Am. Chem. Soc.* **2002**, *124*, 3826−3827.
(19) Aspects of this work have previously been communicated: Lee, D.; Swager, T. M. *J. Am. Chem. Soc.* **2003**, *125*, 6870−6871.
(20) Pangborn, A. B.; Giardello, M. A.; Grubbs, R. H.; Rosen, R. K.; Timmers, F. J. *Organometallics* **1996**, *15*, 1518−1520.
(21) Novak, B. H.; Lash, T. D. *J. Org. Chem.* **1998**, *63*, 3998−4010.

(±)-8-Benzenesulfonyl-9-chloro-4-phenyl-4-azatricyclo[5.2.1.0^{2,6}]-decane-3,5-dione (3). To a rapidly stirred $CHCl_3$ solution (100 mL) of **2** (2.86 g, 7.45 mmol) at 0 °C was added portionwise *m*CPBA (5.10 g, >16.4 mmol). The heterogeneous mixture was warmed to room temperature, stirred for 1.5 h, and treated with an aqueous solution (20 mL) of Na_2SO_3 (2.07 g, 16.4 mmol). A saturated aqueous solution of $NaHCO_3$ was added, and the organic layer was separated. The aqueous layer was extracted with CH_2Cl_2 (100 mL × 2). The combined extracts were washed with saturated aqueous solutions of $NaHCO_3$ and NaCl, dried over anhydrous $MgSO_4$, and filtered. Volatile fractions were removed and the residual colorless oil was purified on silica (hexanes:EtOAc = 1:1) to provide an off-white shiny solid of **3** (2.33 g, 75%). dec 95 °C. ^{1}H NMR (300 MHz, $CDCl_3$): δ 7.92−7.90 (m, 2H), 7.73−7.68 (m, 1H), 7.63−7.58 (m, 2H), 7.48−7.39 (m, 3H), 7.28−7.24 (m, 2H), 4.79 (m, 1H), 3.54 (dd, 1H, J = 4.1 and 5.4 Hz), 3.40−3.24 (m, 4H), 2.51 (d, 1H, J = 11.1 Hz), 3.69 (d, 1H, J = 11.4 Hz). ^{13}C NMR (75 MHz, $CDCl_3$): δ 174.5, 174.0, 137.4, 134.6, 131.7, 129.8, 129.3, 128.9, 128.5, 126.4, 70.4, 56.5, 48.7, 47.3, 46.3, 42.1, 40.9. IR (KBr, cm^{-1}) 3063, 2988, 1773, 1712, 1498, 1447, 1374, 1310, 1181, 1152, 1085, 747, 731, 689, 612, 586. HR-MS (ESI) calcd for $C_{21}H_{18}NO_4ClNaS$ $[M + Na]^+$ 438.0543, found 438.0520.

(±)-8-Benzenesulfonyl-4-phenyl-4-azatricyclo[5.2.1.0^{2,6}]dec-8-ene-3,5-dione (4). A portion of 1,8-diazabicyclo[5.4.0]undec-7-ene (DBU) (600 μL, 4.01 mmol) was added dropwise to a stirred anhydrous CH_2Cl_2 solution (10 mL) of **3** (1.02 g, 2.45 mmol) at 0 °C under Ar. The solution was stirred at 0 °C for 1 h and warmed to room temperature overnight. An aqueous solution of HCl (2 N, 10 mL) was added, and the organic layer was separated. The aqueous layer was extracted with CH_2Cl_2 (30 mL × 2), and the combined extracts were washed with saturated aqueous solutions of $NaHCO_3$ and NaCl, dried over anhydrous $MgSO_4$, and filtered. Volatile fractions were removed to afford **4** as an off-white shiny solid (0.830 g, 91%). mp 206 °C. ^{1}H NMR (300 MHz, $CDCl_3$): δ 7.87−7.83 (m, 2H), 7.57 (tt, 1H, J = 7.5 and 1.1 Hz), 7.46−7.26 (m, 7H), 7.07 (s, 1H), 3.65−3.60 (m, 3H), 3.50 (m, 1H), 1.90 (d, 1H, J = 9.0 Hz), 1.72 (d, 1H, J = 9.3 Hz). ^{13}C NMR (75 MHz, $CDCl_3$): δ 175.1, 173.6, 149.7, 144.2, 138.8, 133.9, 131.6, 129.4, 129.1, 128.6, 128.2, 126.7, 55.3, 46.8, 46.7, 45.8, 45.7. IR (KBr, cm^{-1}) 3065, 2998, 1776, 1713, 1500, 1447, 1378, 1319, 1307, 1186, 1166, 1146, 1089, 129, 719, 690, 624, 596. HR-MS (ESI) calcd for $C_{21}H_{17}NO_4NaS$ $[M + Na]^+$ 402.0776, found 402.0754.

(±)-4-Phenyl-4,10-diazatetracyclo[5.5.1.0^{2,6}.0^{8,12}]tridec-8,11-diene-3,5-dione-9-carboxylic Acid *tert*-Butyl Ester (5). To an anhydrous THF (250 mL) suspension of **4** (11.64 g, 30.7 mmol) under Ar was added *tert*-butyl α-isocyanoacetate (6.98 g, 49.5 mmol). The heterogeneous mixture was placed in an ice bath. A THF solution of ^{t}BuOK (1.0 M, 46 mL) was delivered using a syringe. The reaction mixture was warmed to room temperature and heated at reflux under Ar for 24 h. A saturated aqueous solution of NaCl was added, and the biphasic mixture was concentrated to ca. half its initial volume. The mixture was extracted with CH_2Cl_2 (200 mL × 3), and the combined extracts were dried over Na_2SO_4, filtered, and concentrated to an orange-red oil. Purification on silica (hexanes:EtOAc = 2:1 to 1:1) afforded **5** (9.30 g, 80%) as a pale ivory solid. mp 95 °C. ^{1}H NMR (300 MHz, $CDCl_3$): δ 9.07 (s, 1H), 7.27−7.21 (m, 3H), 6.65−6.61 (m, 2H), 6.58 (d, 1H, J = 2.7 Hz), 4.09 (m, 1H), 3.84 (m, 1H), 3.60−3.57 (m, 2H), 2.27 (d, 1H, J = 9.3 Hz), 2.09 (d, 1H, J = 9.0 Hz), 1.57 (s, 9H). ^{13}C NMR (75 MHz, $CDCl_3$): δ 176.0, 174.9, 160.3, 133.3, 131.3, 129.2, 128.7, 128.1, 126.0, 116.5, 113.9, 81.0, 54.2, 48.9, 48.3, 42.6, 41.8, 28.2. IR (KBr, cm^{-1}) 3298, 2977, 1773, 1713, 1499, 1404, 1369, 1183, 1149, 1108, 732, 691. HR-MS (ESI) calcd for $C_{22}H_{22}N_2O_4Na$ $[M + Na]^+$ 401.1477, found 401.1467.

(±)-4-Phenyl-4,10-diazatetracyclo[5.5.1.0^{2,6}.0^{8,12}]tridec-8,11-diene-3,5-dione-9-carboxylic Acid (6). A portion of **5** (4.37 g, 11.5 mmol) was placed under Ar and treated with trifluoroacetic acid (TFA) (20 mL) with stirring. The resulting pale yellow solution was stirred at room temperature under Ar for 15 min. Volatile fractions were removed, and the residual oily material was suspended in Et_2O (250 mL) to induce precipitation. An off-white solid of **6** (3.71 g, 11.5 mmol, >99%) was isolated by filtration, washed repeatedly with Et_2O, and dried in vacuo. dec 230 °C. ^{1}H NMR (300 MHz, CD_3OD): δ 10.84 (s, 1H), 7.32−7.26 (m, 3H), 6.65−6.61 (m, 3H), 4.36 (d, 1H, J = 4.2 Hz), 3.75 (m, 1H), 3.69−3.62 (m, 2H), 2.20 (d, 1H, J = 9.0 Hz), 2.14 (d, 1H, J = 9.0 Hz). ^{13}C NMR (75 MHz, CD_3OD): δ 178.9, 178.1, 163.9, 136.5, 133.3, 130.8, 129.8, 129.5, 128.0, 116.6, 116.1, 55.5, 50.5, 50.1, 44.0, 43.2. IR (KBr, cm^{-1}) 3293, 3070, 1772, 1694, 1595, 1497, 1456, 1423, 1387, 1286, 1261, 1238, 1201, 1178, 1150, 1129, 1109, 757, 731, 690, 616. HR-MS (ESI) calcd for $C_{18}H_{14}N_2O_4Na$ $[M + Na]^+$ 345.0851, found 345.0858.

2-*endo*,6-*endo*-4-Phenyl-4,10-diazatetracyclo[5.5.1.0^{2,6}.0^{8,12}]-tridec-8,11-diene-3,5-dione (7). An ethylene glycol (70 mL) suspension of **6** (3.20 g, 9.92 mmol), LiCl (4.31 g, 102 mmol), and H_2O (200 mg, 11.1 mmol) was purged with Ar for 15 min. The mixture was placed in a preheated oil bath (190 °C), heated at reflux under Ar for 2 h, and cooled to room temperature. A saturated aqueous solution of NaCl (50 mL) was added, and the organic layer was extracted with Et_2O (200 mL × 3). The combined extracts were washed twice with saturated aqueous NaCl, dried over Na_2SO_4, and filtered. Volatile fractions were removed and the residual solid was recrystallized from boiling hexanes/EtOAc to afford **7** (1.98 g, 7.1 mmol, 72%) as an off-white crystalline material. mp 200 °C. ^{1}H NMR (300 MHz, CD_2Cl_2): δ 8.07 (s, 1H), 7.34 (m, 3H), 6.67 (m, 2H), 6.51 (s, 2H), 3.84 (s, 2H), 3.57 (m, 2H), 2.22 (d, 1H, J = 9.0 Hz), 2.12 (d, 1H, J = 9.0 H). ^{13}C NMR (75 MHz, CD_2Cl_2): δ 176.9, 132.6, 129.2, 128.7, 128.1, 127.1, 109.7, 54.9, 49.8, 42.2. IR (KBr, cm^{-1}) 3370, 2989, 1770, 1705, 1498, 1383, 1188, 1153, 1044, 729, 692. HR-MS (ESI) calcd for $C_{17}H_{15}N_2O_2$ $[M + H]^+$ 279.1133, found 279.1130.

2-*exo*,6-*exo*-4-Phenyl-4,10-diazatetracyclo[5.5.1.0^{2,6}.0^{8,12}]tridec-8,11-diene-3,5-dione (7′). This compound was prepared from 2-*exo*,6-*exo*-4-phenyl-4-azatricyclo[5.2.1.0^{2,6}]dec-8-ene-3,5-dione (= exo isomer of **1**) by a procedure analogous to that used to obtain **7** (overall yield = 40%). mp 248 °C. ^{1}H NMR (300 MHz, DMSO-d_6): δ 10.17 (s, 1H), 7.54−7.41 (m, 3H), 7.29−7.26 (m, 2H), 6.51 (d, 2H, J = 2.1 Hz), 3.57 (s, 2H), 2.84 (s, 2H), 1.86 (d, 1H, J = 10.8 Hz), 1.82 (d, 1H, J = 10.8 Hz). ^{13}C NMR (75 MHz, DMSO-d_6): δ 176.9, 132.3, 130.3, 129.0, 128.5, 127.0, 108.0, 51.1, 46.2, 41.3. IR (KBr, cm^{-1}) 3401, 2991, 2868, 1768, 1705, 1598, 1495, 1381, 1199, 1181, 1149, 1104, 1145, 815, 755, 692, 600. HR-MS (ESI) calcd for $C_{17}H_{14}N_2O_2Na$ $[M + Na]^+$ 301.0947, found 301.0940.

X-ray Crystallographic Studies. Intensity data were collected on a Bruker (formerly Siemens) CCD diffractometer with graphite-monochromated Mo Kα radiation (λ = 0.710 73 Å), controlled by a Pentium-based PC running the SMART software package.[22] Single crystals were mounted at room temperature on the tips of glass fibers, coated with Paraton-N oil, and cooled to 193 K under a cold stream of nitrogen maintained by a Bruker LT-2A nitrogen cryostat. Empirical absorption corrections were applied with SADABS,[23] part of the SHELXTL program package.[24] The possibility of higher symmetry was checked by the program

(22) *SMART v5.05: Software for the CCD Detector System*, version 5.05; Bruker AXS: Madison, WI, 1998.
(23) Sheldrick, G. M. *SADABS: Area-Detector Absorption Correction*; University of Göttingen: Göttingen, Germany, 1996.

PLATON.[25] All non-hydrogen atoms were refined anisotropically unless otherwise noted. Hydrogen atoms were assigned idealized positions and given thermal parameters equivalent to 1.2 times the thermal parameter of the carbon atom to which they are attached. The hydrogen atoms associated with the N−H groups were located in the difference Fourier map and refined isotropically.

Electrochemistry. Electrochemical studies were carried out under ambient conditions with an Autolab Model PGSTAT20 potentiostat (Eco Chemie). A three-electrode configuration consisting of either a platinum button or a 5-μm interdigitated microelectrode as the working electrode, a $Ag/AgNO_3$ (0.01 M in MeCN with 0.1 M (n-Bu_4N)PF_6) reference electrode, and a platinum coil counter electrode was used. The supporting electrolyte was 0.1 M (n-Bu_4N)PF_6 in MeCN. For electrochemistry in aqueous media, a saturated calomel electrode (SCE) and 0.1 M $LiClO_4$ electrolyte were used. Buffer solutions (10 mM) were prepared with citrate (pH 3.0−5.0), phosphate (pH 6.0−8.0), or CHES (pH 9.0). All electrochemical potentials are reported to the Cp_2Fe/Cp_2Fe^+ redox couple unless otherwise noted. Films of poly(**7**) on interdigitated microelectrodes were grown by repeated potential sweeps between −0.5 and +1.2 V (vs Ag/Ag^+) of a monomer solution (7.5 mM) at room temperature. Films of poly(**7′**) were similarly prepared from a monomer solution at 0 °C. The polymer-modified electrode was rinsed with fresh electrolyte solutions and placed in a monomer-free solution. Drain current measurements were typically conducted with a scan rate of 5 mV/s and an offset potential of 40 mV between the two working electrodes. Thickness of the film was determined using a Tencor P10 Surface Profilometer. An average value obtained by three independent measurements was used to calculate the conductivity (σ) of the film.[26,27]

UV−vis Spectroelectrochemistry. In situ spectroelectrochemical measurements were carried out with a UV−vis quartz cuvette using an ITO/glass working electrode (100 Ω/square), a platinum mesh counter electrode, and a $Ag/AgNO_3$ (0.01 M in MeCN with 0.1 M (n-Bu_4N)PF_6) reference electrode. Films were grown on the surface of the working electrode under ambient conditions and washed with fresh electrolyte solutions. The polymer-modified electrode was transferred to a cuvette containing fresh electrolyte, and the UV−vis spectra were taken at 100 mV intervals from the fully reduced form to the fully oxidized form of the polymer.

Results

Monomer Synthesis and Structural Characterization. Synthetic routes to the sterically hindered pyrrole derivatives **7** and **7′** are outlined in Scheme 3. The ring-fused backbone of compound **1** was constructed by a high-yielding Diels−Alder reaction between *N*-phenylmaleimide and cyclopentadiene at 0 °C, which exclusively afforded the kinetic endo adduct.[28] Alternatively, the Diels−Alder adduct of maleic anhydride and cyclopentadiene could be condensed with aniline to afford **1**.[29] The conversion of **1** to a Michael acceptor **4** required three additional steps,[30] each proceeding

Scheme 3. Synthetic Routes to Bicyclo[2.2.1]heptane-Fused Pyrroles

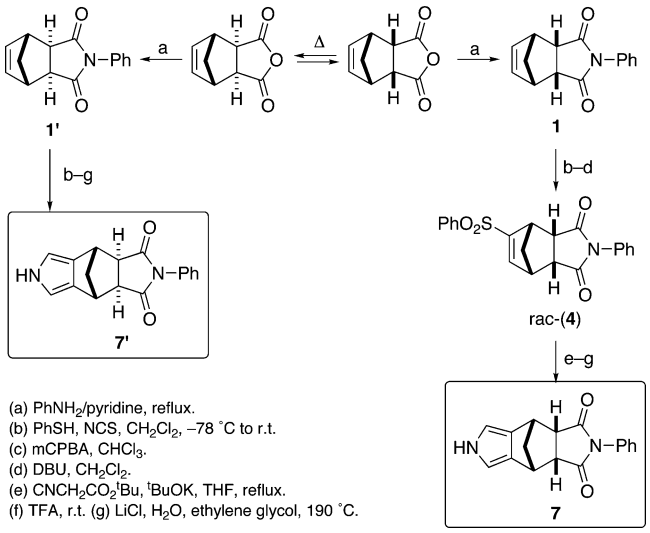

in respectable yield. Following a modified Barton−Zard approach,[31−34] the desired α-substituted pyrrole was constructed with deprotonated *tert*-butyl α-isocyanoacetate as a nucleophile. Acidic cleavage of the *tert*-butyl group, followed by decarboxylation at elevated temperatures, completed the synthesis of the phenyl-canopied pyrrole **7**.

Synthesis of the *exo*-pyrrole **7′** commenced with a thermal isomerization of the initial kinetic Diels−Alder adduct of maleic anhydride and cyclopentadiene (Scheme 3).[35] The exo isomer was separated and subjected to a reaction with aniline in refluxing pyridine.[29] The condensation product, **1′**, a formal exo adduct of *N*-phenylmaleimide and cyclopentadiene, was converted to **7′** in six steps, in a manner similar to that described for the synthesis of **7** (overall yield = 40%).

The solid-state structures of **7** and **7′** were determined by X-ray crystallography. As shown in Figure 1, the pendant

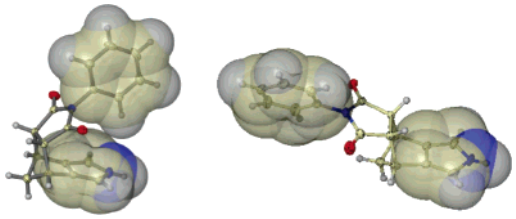

Figure 1. Solid-state structure of **7** (left) and **7′** (right) determined by X-ray crystallography. Overlaid on the thermal ellipsoids (50% probability) are space-filling representations of the pyrrolic and phenyl fragments of each molecule.

phenyl groups in **7** and **7′** are canted with respect to the plane defined by the diimide fragment, with the $C_{\beta-phenyl}-C_{\alpha-phenyl}-N-C_{\alpha-carbonyl}$ torsional angles ranging from 62 to 81°. Such a conformation apparently alleviates the steric crowding between the phenyl hydrogen atoms and the carbonyl lone pair electrons. In the crystal packing diagrams,

(24) Sheldrick, G. M. *SHELXTL97-2: Program for the Refinement of Crystal Structures*; University of Göttingen: Göttingen, Germany, 1997.
(25) Spek, A. L. *PLATON, A Multipurpose Crystallographic Tool*; Utrecht University: Utrecht, The Netherlands, 1998.
(26) Zotti, G.; Schiavon, G. *Synth. Met.* **1990**, *39*, 183−190.
(27) Kingsborough, R. P.; Swager, T. M. *J. Am. Chem. Soc.* **1999**, *121*, 8825−8834.
(28) Harvey, S. C. *J. Am. Chem. Soc.* **1949**, *71*, 1121−1122.
(29) Abbady, M. S.; Kandeel, M. M.; Youssef, M. S. K. *Phosphorus, Sulfur, Silicon* **2000**, *163*, 55−64.
(30) Hopkins, P. B.; Fuchs, P. L. *J. Org. Chem.* **1978**, *43*, 1208−1217.
(31) Barton, D. H. R.; Zard, S. Z. *J. Chem. Soc., Chem. Commun.* **1985**, 1098−1100.
(32) Barton, D. H. R.; Kervagoret, J.; Zard, S. Z. *Tetrahedron* **1990**, *46*, 7587−7598.
(33) Abel, Y.; Montforts, F.-P. *Tetrahedron Lett.* **1997**, *38*, 1745−1748.
(34) Abel, Y.; Haake, E.; Haake, G.; Schmidt, W.; Struve, D.; Walter, A.; Montforts, F.-P. *Helv. Chim. Acta* **1998**, *81*, 1978−1996.
(35) Craig, D. *J. Am. Chem. Soc.* **1951**, *73*, 4889−4892.

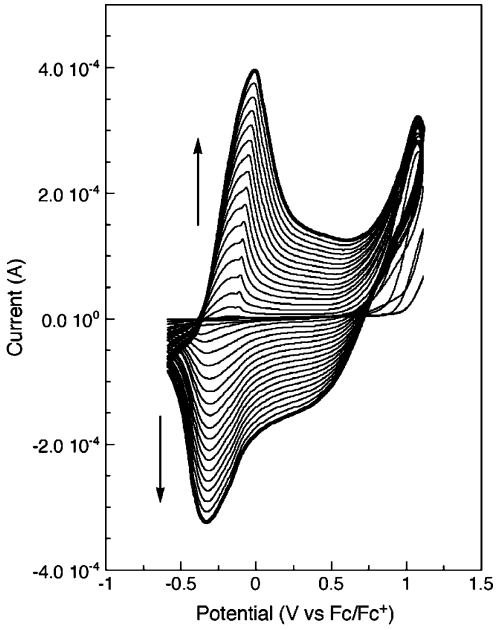

Figure 2. Anodic polymerization of **7** on a 5-μm interdigitated Pt electrode in MeCN with 0.1 M (n-Bu_4N)PF_6 as supporting electrolyte and a scan rate of 100 mV/s at 25 °C.

hydrogen-bonding interactions between the pyrrolic N−H groups and the imide C═O groups were identified with the N−H···O distances of 2.885(4)−3.067(3) Å.

Electropolymerization. To determine appropriate potential windows for anodic polymerization, electrochemical properties of **7** and **7′** were investigated by cyclic voltammetry (CV). Cyclic voltammograms of a MeCN solution of the endo isomer **7** revealed an oxidation peak at 1130 mV,[36] which does not display a corresponding reduction wave in the return sweep. Under identical conditions, the exo isomer **7′** exhibited a similarly irreversible oxidation process at +950 mV.

Anodic polymerization of **7** proceeds best in MeCN doped with H_2O (0.3%, v/v). As shown in Figure 2, a well-defined redox couple centered at −175 mV developed upon repeated potential cycling between −0.5 and +1.2 V vs Ag/Ag^+. A linear dependence of the peak current on the scan rate unambiguously established that this redox activity arises from surface-bound poly(**7**), the conductivity of which increased upon oxidation and maximized at −90 mV ($\sigma_{max} \approx 40$ S cm^{-1}).[19] Under similar conditions, initial attempts to electropolymerize **7′** failed. Dark green streaks generated during positive potential sweeps readily diffused away from the electrode surface, as visually inspected. Reproducible deposition of poly(**7′**), however, was aided by conducting polymerization reactions at 0 °C (Figure S1, Supporting Information). Films of poly(**7′**) thus prepared display a narrow range of high conductivity ($\sigma_{max} \approx 12$ S cm^{-1}) centered at −95 mV in MeCN (Figure 3). The potential−conductivity profile of poly(**7′**) correlates well with the changes in CV currents in both the oxidative and reductive potential sweeps. Essentially identical behavior displayed by poly(**7**) implies that similar charge-transporting mechanisms are operative for both polypyrrole derivatives, in which appended phenyl groups help suppress interchain electronic coupling.[19]

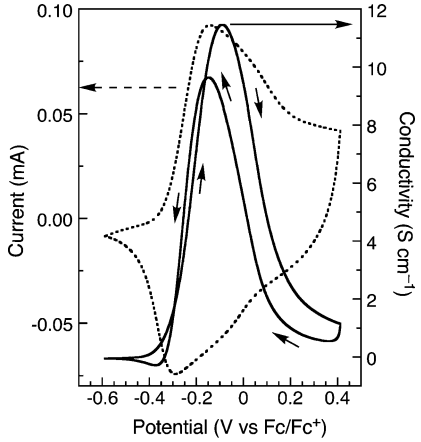

Figure 3. Cyclic voltammogram (50 mV/s; dotted line) and in situ conductivity measurement (5 mV/s, offset potential of 40 mV; solid line) of poly(**7′**) on 5-μm interdigitated Pt electrodes in MeCN with 0.1 M (Bu_4N)PF_6 as supporting electrolyte (T = 0 °C).

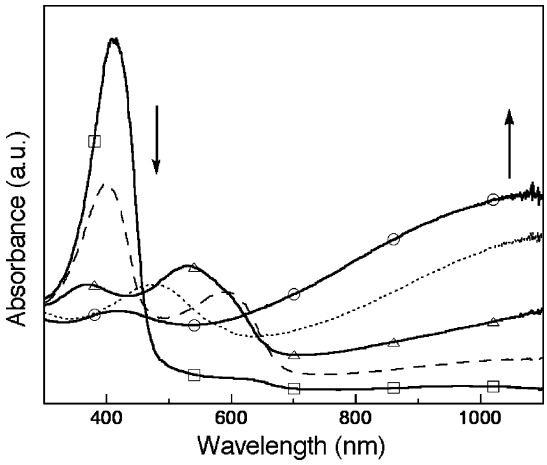

Figure 4. Electronic absorption spectra of poly(**7**) on ITO-coated glass electrodes in MeCN with 0.1 M (Bu_4N)PF_6 as supporting electrolyte measured at −350 (−□−), −150 (---), 0 (−△−), +300 (···), and +800 mV (−○−) vs Ag/Ag^+ (0.01 M).

Spectroelectrochemistry. UV−vis spectra of poly(**7**) deposited on ITO-coated glass electrodes were obtained as a function of applied potential. A yellow film of poly(**7**) in its fully reduced state (E = −350 mV vs Ag/Ag^+) displays a sharp absorption at 420 nm (Figure 4). This interband transition rapidly decays upon oxidation of the material. A concomitant buildup of longer wavelength transitions associated with the polaronic and bipolaronic states were observed at 620 and >1100 nm, respectively, similar to the observations made with the parent unsubstituted polypyrrole system.[37−40] With increase in the doping level, features arising from the polaronic state gradually diminish. At the positive end of the potential scan (+800 mV vs Ag/Ag^+), the UV−vis spectrum of poly(**7**) is dominated by a broad near-IR absorption associated with the bipolaronic state. Evolution of the cation radicals in doped poly(**7**) was traced

(36) All potentials are referenced to Fc/Fc^+ unless otherwise noted.
(37) Kaufman, J. H.; Colaneri, N.; Scott, J. C.; Street, G. B. *Phys. Rev. Lett.* **1984**, *53*, 1005−1008.
(38) Zotti, G.; Schiavon, G. *Synth. Met.* **1989**, *30*, 151−158.
(39) Amemiya, T.; Hashimoto, K.; Fujishima, A. *J. Electrochem. Soc.* **1991**, *138*, 2845−2850.
(40) Son, Y.; Rajeshwar, K. *J. Chem. Soc., Faraday Trans.* **1992**, *88*, 605−610.

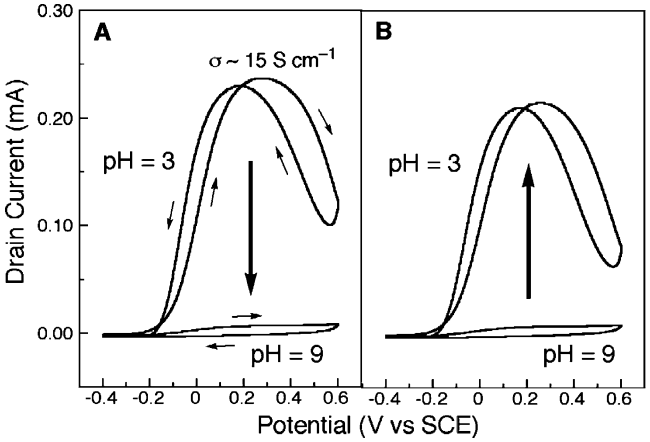

Figure 5. In situ conductivity measurement (5 mV/s, offset potential of 40 mV) of poly(**7**) on 5-μm interdigitated Pt electrodes in H_2O at pH 3 (citrate buffer, 10 mM) and at pH 9 (CHES buffer, 10 mM) with 0.1 M $LiClO_4$ as supporting electrolyte (A), and recovery of conductivity after switching from pH 9 to pH 3 (B).

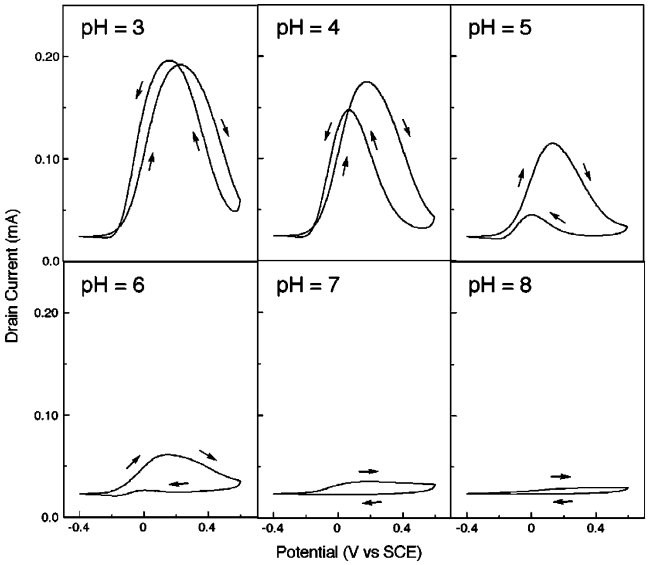

Figure 6. In situ conductivity measurements (5 mV/s, offset potential of 40 mV) of poly(**7**) on 5-μm interdigitated Pt electrodes between pH 3 and pH 8 ([$LiClO_4$] = 0.1 M; [buffer] = 10 mM).

further by in situ EPR spectroscopy. The buildup and decay of the $S = 1/2$ ground spin state species as monitored by the EPR signal at $g = 2.00$ match closely the changes in the CV current as well as conductivity.[19] Essentially identical spin counts were obtained in the oxidative and reductive potential sweeps.

Protonic Doping in Aqueous Media. In aqueous electrolytes at pH 3, poly(**7**) deposited on Pt interdigitated microelectrodes provides reproducible cyclic voltammograms and conductivity profiles upon repeated potential sweeps. As shown in Figure 5A, the conductivity of poly(**7**) increases with oxidation and maximizes at ~15 S cm^{-1}. Further oxidation results in a decrease, defining finite potential windows of high conductivity centered at +280 mV (vs SCE). An essentially identical bell-shaped potential−conductivity profile was obtained in the return sweep, with a cathodic shift by ca. 100 mV compared with the oxidative sweep. Upon exposure to electrolyte solutions at pH 9, both the cyclic voltammograms and conductivity profiles of poly(**7**) became almost featureless (Figures 5A and S2), with a significant drop in conductivity (>97% as measured at +280 mV). The conductivity, as well as the redox activity, of the material, however, was recovered upon reexposure to an aqueous media at pH 3 (Figures 5B and S2). In stark contrast to the excellent stability of poly(**7**), which retains its electroactivity after repeated cycling between acidic and basic aqueous media, poly(**7′**) subjected to similar conditions exhibits substantial decay in its charge-carrying ability. After five scans at pH 3, the σ_{max} of poly(**7′**) decreased to ca. 25% of its initial value (Figure S3).[41]

The excellent reversibility of poly(**7**) led us to map out a detailed pH−conductivity profile of this material. As shown in Figure 6, two salient features emerge as the electrolyte pH is increased from 3 to 8: the maximum conductivity (σ_{max}) of poly(**7**) gradually decreases and the hysteresis between positive and negative potential sweeps becomes more pronounced.

Discussion

Monomer Design, Synthesis, and Electropolymerization. Sterically hindered pyrrole derivatives having polycyclic backbones have precedents in porphyrin literature. Notable examples include triptycene-type pyrroles that afforded rigid biconcave porphyrins after condensation with suitable aldehydes and subsequent oxidation.[42,43] The pyrrolic fragments in these conformationally well-defined compounds and their analogues were accessed either by reduction and subsequent hydrolysis[42,43] of dinitriles or by reactions between deprotonated α-isocyanoesters and electron-deficient olefins.[44−48]

In addition to increasing the structural dimensionality of the planar precursor, installation of polycyclic skeletons on the β-positions of pyrrole enhances chemical stability by suppressing the activation of exocyclic C−H bonds or electrophilic attack on the pyrrole ring. We reasoned that a more effective steric shielding, a key architectural requirement to minimize interstrand $\pi-\pi$ stacking interactions in the resulting polypyrrole derivative, could be achieved by positioning insulating organic groups directly above the pyrrole ring. A modular approach for the target molecules was also desired in order to facilitate modification of both steric and electronic demands of the canopy unit if necessary.[49]

(41) As shown in Figure S3, a large hysteresis was observed in the conductivity profile of poly(**7′**) in oxidative and reductive potential sweeps at pH 3, indicating a significant structural reorganization upon removal and injection of electrons. Repeated potential scans resulted in a rapid decay of the conductivity of poly(**7′**), preventing further studies.

(42) Ramondenc, Y.; Schwenninger, R.; Phan, T.; Gruber, K.; Kratky, C.; Kräutler, B. *Angew. Chem., Int. Ed. Engl.* **1994**, *33*, 889−891.
(43) Schlögl, J.; Kräutler, B. *Synlett* **1999**, 969−971.
(44) Ito, S.; Murashima, T.; Ono, N. *J. Chem. Soc., Perkin Trans. 1* **1997**, 3161−3165.
(45) Ito, S.; Uno, H.; Murashima, T.; Ono, N. *Chem. Commun.* **1999**, 2275−2276.
(46) Ito, S.; Ochi, N.; Uno, H.; Murashima, T.; Ono, N. *Chem. Commun.* **2000**, 893−894.
(47) Ito, S.; Uno, H.; Murashima, T.; Ono, N. *Tetrahedron Lett.* **2001**, *42*, 45−47.
(48) Ito, S.; Watanabe, H.; Uno, H.; Murashima, T.; Ono, N.; Tsai, Y. C.; Compton, R. G. *Tetrahedron Lett.* **2001**, *42*, 707−710.

Synthetic routes outlined in Scheme 3 were thus devised and successfully implemented. Here, Diels−Alder adducts of cyclopentadiene and maleimide/maleic anhydride served as readily accessible and conformationally rigid platforms, which could be elaborated further to integrate phenyl and pyrrole fragments. The endo/exo stereoisomerism of the initial adduct dictates the relative positioning of the canopy unit in the C-shaped (from endo) or Z-shaped (from exo) pyrrole product, as unambiguously determined by crystallographic chemical analysis of **7** and **7′** (Figure 1).

Polypyrroles afforded by **7** and **7′** thus have compositionally identical monomer units and display similar bell-shaped potential−conductivity profiles in MeCN, indicating that polaronic charge carriers are responsible for the electrical conductivity of both materials. Despite such similarity, however, poly(**7**) and poly(**7′**) exhibit markedly different electrochemical stabilities. Poly(**7**), having phenyl groups placed directly above the CP chain, can be reversibly switched between its conductive and insulating states, whereas poly(**7′**), having identical elemental composition with the phenyl pendants positioned away from the CP chain, is apparently susceptible to irreversible structural and/or chemical transformations. This instability most likely prevents the reversibility of the protonation and deprotonation of the polymer backbone, which is reflected by the substantial decay in conductivity upon repeated doping and dedoping. Although a detailed understanding of this process is beyond the scope of this investigation, the electrochemical stability of the present system is substantially affected by the monomer stereochemistry, which controls the immediate space around the CP chains. This finding also points toward the importance of chemical structure in dictating the properties of CPs.

Polaron Migration and Protonic Doping. The paradigm of an interdependent tuning of conductivity by oxidative and protonic doping has been established for polyanilines.[50−52] Specifically, treatment of emeraldine base, a partially p-doped form of the neutral precursor, with Brønsted acids (pH $<\sim$0) was accompanied by a 9−10 order of magnitude increase in conductivity.[50] The contribution of the polysemiquinone radical cation character to the protonated emeraldine salt leads to an extensive spin and charge delocalization along the polyaniline backbone. A conceptually parallel process has recently been noted for a proton-doped CP having extended *p*-dihydroquinone segments.[53,54] Related examples are also found in the unsubstituted polypyrrole system, in which deprotonation of the N−H groups in oxidized polymer and the accompanying decrease in conductivity have been investigated.[55−57]

Scheme 4. Proton-Coupled Redox Chemistry

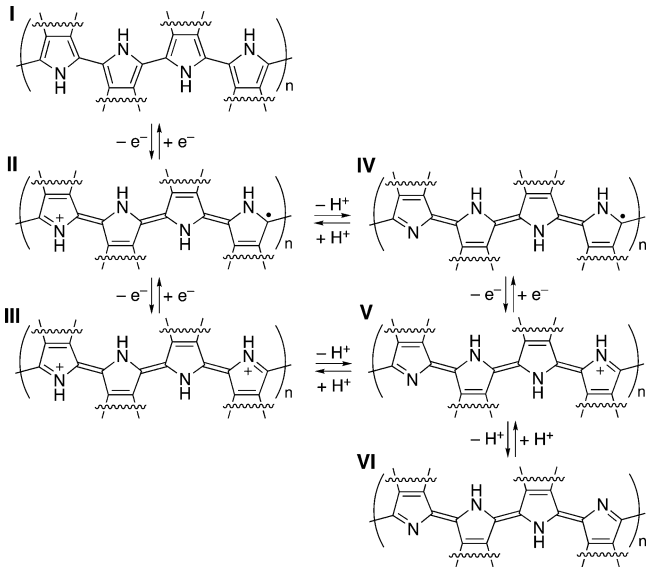

We previously communicated the unusually narrow potential windows of high conductivity exhibited by poly(**7**) in MeCN electrolytes.[19] An excellent correlation between the conductivity and the potential-dependent change in the amount of $S = 1/2$ spin state species, as probed by in situ EPR spectroscopy, fully established that charge-delocalized cation radicals (polarons) are major participants in the charge-carrying mechanism of oxidatively doped poly(**7**). This notion was further corroborated by UV−vis spectroelectrochemical studies.

As summarized in Scheme 4, oxidation of neutral poly(**7**) (**I**) successively generates p-doped polaronic (**II**) and bipolaronic (**III**) states. Shuttling within the **I**−**II**−**III** redox cycle does not involve any acid−base chemistry and affords a conductivity profile that maximizes at the highest concentration of the polaronic state **II**. Little hysteresis in the conductivity profile is thus expected in the oxidative and reductive scans. This model is consistent with the electrochemical properties of poly(**7**) at pH 3 (Figures 5 and 6). Despite a decrease in the pK_a value of the pyrrolic N−H groups of the increasingly charged polymer in the polaronic state, poly(**7**) apparently retains its proton inventory at this low pH end. Consequently, an essentially identical σ_{max} is obtained in the return sweep, as **III** takes up electrons to revert to **II** and subsequently to **I**.

Loss of iminium protons from **II** and **III** at higher pH, however, affords neutral residues having contributions from quinoid structures (**IV**, **V**, and **VI**). Migration of charge carriers now becomes energetically less favorable due to the lack of resonance stabilization of the key cation radical. With increasing [OH^-], contributions from **IV**−**VI** become dominant in the polymer redox cycle. The concomitant decrease in the amount of **II** results in significantly lowered conductivity in the oxidative scan at higher pH. As bipolarons (**III**) that still retain their iminium protons can take up electrons to become **II** in the reductive scan, the hysteresis in the

(49) For example, a 2-pyridyl analogue of **7** could be prepared, in which a potential metal-binding site is installed directly above the pyrrole group.
(50) Chiang, J.-C.; MacDiarmid, A. G. *Synth. Met.* **1986**, *13*, 193−205.
(51) MacDiarmid, A. G.; Epstein, A. J. *Faraday Discuss. Chem. Soc.* **1989**, *88*, 317−332.
(52) MacDiarmid, A. G. *Angew. Chem., Int. Ed.* **2001**, *40*, 2581−2590.
(53) Yu, H.-h.; Xu, B.; Swager, T. M. *J. Am. Chem. Soc.* **2003**, *125*, 1142−1143.
(54) Yu, H.-h.; Pullen, A. E.; Büschel, M. G.; Swager, T. M. *Angew. Chem., Int. Ed.* **2004**, *43*, 3700−3703.
(55) Inganäs, O.; Erlandsson, R.; Nylander, C.; Lundström, I. *J. Phys. Chem. Solids* **1984**, *45*, 427−432.
(56) Nishizawa, M.; Matsue, T.; Uchida, I. *Anal. Chem.* **1992**, *64*, 2642−2644.
(57) Talaie, A. *Polymer* **1997**, *38*, 1145−1150.

forward and backward sweeps becomes more pronounced with increasing pH (Figure 6). The canopy is key to this reversibility as it limits interchain associations that can lead to structural evolutions that disfavor reversible protonation and deprotonation. In addition, it creates a more open structure that more readily allows for hydroxides and protons to approach the polypyrrole iminium/imine groups. As mentioned earlier, the effective isolated structure of the polymer backbones also yields greater sensitivity to the creation of defects.[19]

Summary and Perspectives

Conformationally rigid canopied pyrrole derivatives were designed to assemble electroactive materials having limited interstrand electronic coupling. By adding structural dimensionality to typically planar polypyrrole backbone, the dimensionality of the charge hopping pathways responsible for conduction was effectively lowered. The canopied structure provides for fast and reversible response kinetics in pH responses. The bicyclo[2.2.1]hepane-fused maleimide scaffold we have explored can position a diverse array of steric and electronic controller groups in close proximity to the polypyrrole backbone, and should facilitate the generation of CPs having potential recognition sites for sensing applications.

Acknowledgment. This work was supported by the Institute for Soldier Nanotechnologies and the ONR. We thank Dr. H.-h. Yu for help in acquiring spectroelectrochemical data and valuable discussions.

Supporting Information Available: Electrochemistry of **7**, **7′**, poly(**7**), and poly(**7′**), and an X-ray crystallographic file (CIF). This material is available free of charge via the Internet at http://pubs.acs.org.

CM050803R